Int. J. Heat Mass Transfer. Vol. 28, No. 8, pp. 1525–1537, 1985
Printed in Great Britain

0017–9310/85 $3.00 + 0.00
Pergamon Press Ltd.

Heat transfer during the early expansion of gas in pressurized vessels

S. PAOLUCCI

Analytical Thermal/Fluid Mechanics Division, Sandia National Laboratories, Livermore, CA 94550, U.S.A.

(*Received* 24 *October* 1984 *and in final form* 31 *January* 1985)

Abstract—We investigate the behavior of a gas in a pressurized container during early expansion for the special case where the outflow is choked. Using a boundary-layer approximation that includes conduction and gas expansion effects we are able to obtain analytical solutions in closed form. A key quantity that determines the subsequent process the gas will go through in later stages of the discharge is the wall heat transfer. From the analytical results we are able to identify the important parameters that govern this early portion of the discharging process, and particularly the heat transfer process.

1. INTRODUCTION

WHEN GAS is permitted to escape freely from a pressurized vessel, the gas that remains in the vessel is considered to undergo an expansion. It is well known that this expansion process is not isentropic for the complete blowdown [1]. However, it is an accepted fact that there is always a period of time, starting from an instantaneous valve opening time, where both the pressure and temperature histories in the core of the vessel closely follow their respective isentropic variations, but eventually depart from them. In this paper we will be concerned exclusively with this initial part of the discharge.

The analysis of this problem was originally treated by Landram [2] and Johnston and Dwyer [3]. Landram gave an approximate solution in which the time-dependent diffusion-layer thickness was obtained using an integral method. His final results were corrected by Johnston and Dwyer and are included in their paper, where they also show that Landram's predicted behavior does not agree with their experimental results. They point out that the reason for the disagreement is that the boundary-layer similarity assumption used by Landram is incorrect. Johnston and Dwyer [3] then go on to obtain numerical solutions to the problem. The behavior of their results generally agrees with their experimental data. It is to be noted that in their numerical solutions, all convective effects are neglected. It is expected that as time evolves, convective effects will become more and more important.

In the present work we include convective effects due to gas expansion near the walls. The aim of this work is to identify the important parameters that govern this early portion of the discharging process, and particularly the heat transfer process. The amount of heat transfer in the early part is a key quantity that determines the subsequent processes the gas will go through in later stages.

In Section 2 we derive the equations, initial and boundary conditions that govern the problem and discuss the approximations made. In Section 3 we obtain explicit analytical solutions to the problem. In Section 4 we discuss the analytical solutions, obtain some specific results, and compare them with available data. We conclude in Section 5 with some comments on the results, and suggestions for further studies.

2. ANALYSIS

A gas initially at a temperature T_0 and pressure p_0 is discharged from a vessel, through a small convergent nozzle, to the ambient which is at a pressure p_a^*, as shown in Fig. 1. We would like to study the behavior of

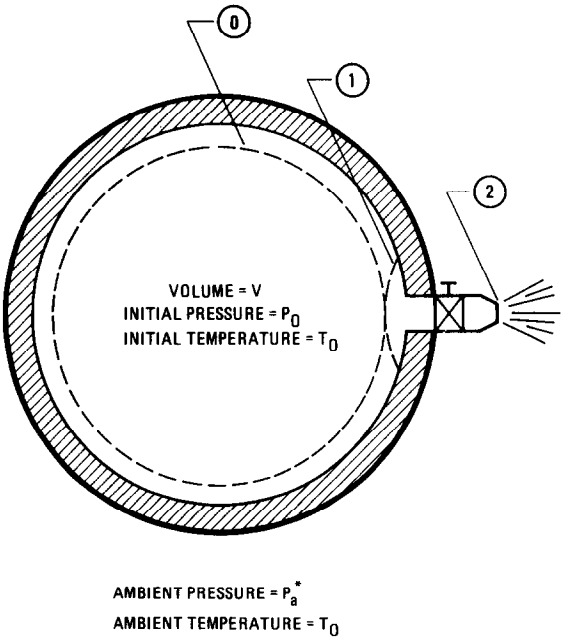

FIG. 1. Regions of different flow behavior during the early time of a discharging vessel.

NOMENCLATURE

c	acoustic speed
c_d	total loss coefficient
c_p	specific heat at constant pressure
c_v	specific heat at constant volume
d	reference length
erf	error function
$erfc$	complementary error function
${}_2F_1$	Gauss' hypergeometric function
Fr	Froude number
g	magnitude of gravitational vector
k	thermal conductivity
K	dummy variable
m	dummy variable
$\dot{m}$	mass flow rate
Ma	Mach number
n_i	normal vector
Nu	Nusselt number
p	pressure
Pe	Péclet number
q	wall heat flux
r	critical pressure ratio
Ra	Rayleigh number
Ra_0	$Re\,Pe/Fr$
Re	Reynolds number
S	surface area
t	time
T	temperature
$\mathscr{T}$	reference time
u	velocity normal to wall
U	reference speed
v_j	velocity vector
V	volume
x	coordinate normal to wall
x_j	coordinates
y	dummy variable
z	dummy variable.

Greek symbols

α	$Pe\left(\frac{\gamma+1}{\gamma-1}\right)$
β	dummy variable
γ	ratio of specific heats
Γ	$\frac{\gamma-1}{\gamma}$, also gamma function
δ	thermal boundary-layer thickness
ε	dummy variable
κ	dummy variable
λ	dummy variable
μ	dynamic viscosity
ν	dummy variable
Π	scaled dynamic pressure
ρ	density
τ	transformed time
τ_{ij}	viscous stress tensor
ϕ	$Tp^{-\Gamma}$
χ	$\phi-1$
ψ	stream coordinate.

Subscripts

a	ambient
w	wall
0	initial
1	surface 1
2	surface 2
∞	outside of boundary layer.

Superscript

*	dimensional quantity.

the heat transferred from the walls to the gas during the initial discharge period.

It has been shown recently [4], using an order-of-magnitude estimate, that the effect of acoustic waves in a discharging vessel is negligible. This results in a pressure variation inside the discharging vessel to be, with excellent accuracy, only a function of time, in accord with the experimental data of Johnston [1]. After filtering acoustic waves, and neglecting radiation effects, it has been shown [4] that the governing dimensionless equations for a perfect gas become

$$\frac{\partial \rho}{\partial t} + \frac{\partial}{\partial x_j}(\rho v_j) = 0, \tag{1}$$

$$\frac{\partial}{\partial t}(\rho v_i) + \frac{\partial}{\partial x_j}(\rho v_j v_i) = -\frac{\partial \Pi}{\partial x_i} + \frac{n_i}{Fr}\rho + \frac{1}{Re}\frac{\partial}{\partial x_j}\tau_{ij}, \tag{2}$$

$$\rho c_p\left(\frac{\partial T}{\partial t} + v_j\frac{\partial T}{\partial x_j}\right) - \Gamma\frac{dp}{dt} = \frac{1}{Pe}\frac{\partial}{\partial x_j}\left(k\frac{\partial T}{\partial x_j}\right), \tag{3}$$

$$p(t) = \rho T, \tag{4}$$

where n_i is a unit vector in the direction of gravity, $\Pi = (Ma^2/\gamma)p^{(1)}$, $p^{(1)}$ is a correction to the static pressure $p(t)$, and accounts for hydrostatic and dynamic effects, and τ_{ij} is the viscous stress tensor. The dimensionless parameters are defined as follows:

$$\Gamma = \frac{\gamma-1}{\gamma}, \quad Fr = \frac{U^2}{gd}, \quad Re = \frac{\rho_0 U d}{\mu_0}, \quad Pe = \frac{\rho_0 c_{p0} U d}{k_0}, \quad Ma = \frac{U}{c_0}, \tag{5}$$

where $\gamma = c_{p0}/c_{v0}$. Zero subscripts denote initial values,

d is a characteristic vessel dimension, and U denotes a reference speed defined by $U = d/\mathscr{T}$. $\mathscr{T}$ is a reference time to be defined shortly. In order to make the variables dimensionless we have used initial data for the characteristic quantities. T_0, ρ_0 and p_0 are scales of temperature, density, and pressure, respectively. The coefficients of viscosity, thermal conductivity, and specific heats are also normalized by their initial values μ_0, k_0, c_{p_0}, and c_{v_0}, respectively. In the following analysis we shall take the specific heats to be constant (i.e. $c_p = 1$ due to the nondimensionalization), and the vessel wall to be isothermal. Also, from here forward, all dimensional quantities will be denoted by a star superscript; all other variables will be understood to be dimensionless.

For convenience, we consider the vessel to be divided into three regions, separated by surfaces 0 and 1. We take the flow of gas in the nozzle region between surfaces 1 and 2 to be one-dimensional. We assume surface 1 to be near enough to the exit that essentially all the gas is to the left of it, but far enough from the exit that the fluid velocity through surface 1 is small. We further assume that the average fluid properties to the left of 1 are equal to those at surface 1. Lastly, we assume that surface 0 is close enough to the walls such that most of the gas is to the inside of it, but far enough from them so that the average fluid properties on 0 are the same as those in the region between 0 and 1.

We will now analyze the three regions separately.

(a) *The nozzle region between surfaces* 1 *and* 2

We will assume for simplicity that the flow between surfaces 1 and 2 is isentropic (i.e. both frictionless and adiabatic). Deviations from this assumption could easily be incorporated through a constant loss coefficient, which would simply modify the definition of the reference time. The behavior of this region of the system is then described by the transient isentropic mechanical energy balance. However, for relatively small vessel openings, the flow can be approximated as one of quasi-steady-state. Then, since the kinetic energy at surface 1 is smaller than that at surface 2 (and hence can be neglected), the resulting Bernoulli equation can be solved to yield the instantaneous mass discharge rate. Under most circumstances we have that $p_a < r$, where p_a is the dimensionless ambient pressure, and $r = [2/(\gamma+1)]^{1/\Gamma}$ is a critical pressure ratio, and thus the flow will be initially choked at surface 2. In the following analysis we will assume that p_a/p_1, where p_1 is the dimensionless pressure in the vessel core, will remain less than r for the period of interest. Our analysis will become invalid when this restriction is violated.

Under the above circumstances, the mass flow rate is given by

$$\dot{m} = \frac{S_2}{Ma}[p_1\rho_1 r^{(\gamma+1)/\gamma}]^{1/2}, \tag{6}$$

where we have chosen the adiabatic reference time given by $\mathscr{T}^{-1} = S_2^* c_0(\gamma-1)r^{(\gamma+1)/2\gamma}/2V^*$ as the characteristic time scale, where S_2^* and V^* are the dimensional opening area at 2 and the vessel volume, respectively, and c_0 is the initial sound speed. Quantities with subscript 1 are evaluated at surface 1.

(b) *The core region between surfaces* 0 *and* 1

Because the velocity of the gas at surface 1 is relatively small, it will be even smaller in the entire core region between surfaces 0 and 1. Hence we neglect the kinetic energy of the gas in comparison to the internal energy. It can also be shown that initially thermal diffusion effects are negligible in the core, and that the thermodynamic field is approximately constant in space, and equal to that on surface 1. Now combining the resulting energy equation with the equations of continuity and state, it can easily be shown that we obtain the following isentropic relations between the thermodynamic properties:

$$T_1 = p_1^{\Gamma}, \quad \rho_1 = p_1^{1/\gamma}, \quad T_1 = \rho_1^{(\gamma-1)}. \tag{7}$$

The results (6) and (7) can now be combined and integrated to obtain expressions with explicit time dependence. That is, we find that

$$T_1 = (1+t)^{-2}, \quad p_1 = (1+t)^{-2/\Gamma}, \quad \rho_1 = (1+t)^{-2/(\gamma-1)}, \tag{8}$$

and the mass flow-rate and the velocity at surface 1 are given by

$$\dot{m} = V\left(\frac{2}{\gamma-1}\right)(1+t)^{-(\gamma+1)/(\gamma-1)}, \quad v_1 = \frac{V}{S_1}\left(\frac{2}{\gamma-1}\right)(1+t)^{-1}, \tag{9}$$

where S_1 is the dimensionless area of surface 1.

(c) *The boundary-layer region between the walls and surface* 0

In the region next to the walls the velocity field is affected by three separate contributions: (1) expansion of gas due to thermodynamic effects; (2) forced convective effects due to the discharging process; and (3) natural convective effects due to the presence of the gravity field. The first contribution always gives rise to a velocity direction normal to the walls. The second contribution gives rise to a negligible component of velocity approximately in the direction of the opening. The third contribution gives rise to a velocity component opposite to the direction of gravity n_i.

In the following analysis we will neglect the third contribution. We will discuss its effect later. We will show that the contribution is typically small compared to that due to expansion of the gas in the early part of the discharge. We neglect the kinetic energy of the gas in comparison to the internal energy, and we also assume that the boundary-layer thickness δ will remain small, through our period of interest, compared to the radius of curvature of the walls (e.g., for a cylinder or sphere $\delta^* \ll d/2$). It can now be shown that the boundary-layer

equations for the gas near the walls, resulting from equations (1)–(4), are given by

$$\frac{\partial \rho}{\partial t} + \frac{\partial}{\partial x}(\rho u) = 0, \tag{10}$$

$$\rho\left(\frac{\partial T}{\partial t} + u\frac{\partial T}{\partial x}\right) = \Gamma\frac{\mathrm{d}p}{\mathrm{d}t} + \frac{1}{Pe}\frac{\partial}{\partial x}\left(k\frac{\partial T}{\partial x}\right), \tag{11}$$

$$p(t) = \rho T, \tag{12}$$

where x measures the normal distance from the walls. Note that by matching with the core we have that the $p(t)$ variation is given by (8) since $p = p_1$ throughout the vessel, and the initial and boundary conditions are

$$T(x,0) = 1, \quad T(0,t) = T_w, \quad T(+\infty,t) = T_1(t). \tag{13}$$

In the above equation $x \to +\infty$ is intended to mean far enough from the walls (i.e. surface 0), and we have allowed for the wall temperature to be different than the initial temperature of the gas.

It has been shown in [4, 5] that by letting $T = p^{\Gamma}\phi$, the energy equation (11) can be written as

$$\rho\left(\frac{\partial \phi}{\partial t} + u\frac{\partial \phi}{\partial x}\right) = \frac{1}{Pe}\frac{\partial}{\partial x}\left(k\frac{\partial \phi}{\partial x}\right). \tag{14}$$

The equation of state now becomes

$$p^{1/\gamma} = \rho\phi. \tag{15}$$

In the same spirit as [5], if we introduce a stream function ψ defined by

$$\rho = \frac{\partial \psi}{\partial x}, \quad \rho u = -\frac{\partial \psi}{\partial t}, \tag{16}$$

so that the continuity equation (10) is identically satisfied, and assume (to a good approximation for many gases) that the thermal conductivity varies linearly with temperature, then equations (14) and (15) can be combined into

$$\frac{\partial \phi}{\partial t} = \frac{p}{Pe}\frac{\partial^2 \phi}{\partial \psi^2}. \tag{17}$$

By rescaling the time by

$$\tau = \frac{1}{Pe}\int_0^t p(t')\,\mathrm{d}t', \tag{18}$$

and letting $\chi = \phi - 1$, equation (17) becomes the standard heat conduction equation

$$\frac{\partial \chi}{\partial \tau} = \frac{\partial^2 \chi}{\partial \psi^2}. \tag{19}$$

The initial and boundary conditions (13) transform into

$$\chi(\psi,0) = 0, \quad \chi(0,\tau) = \chi_0(\tau), \quad \chi(+\infty,\tau) = 0, \tag{20}$$

where

$$\chi_0(\tau) = T_w p^{-\Gamma}(\tau) - 1 = T_w(1-\alpha\tau)^{-2(\gamma-1)/(\gamma+1)} - 1,$$

and $\alpha = Pe(\gamma+1)/(\gamma-1)$.

Note that the region $0 \leqslant x < +\infty$ maps to $0 \leqslant \psi < +\infty$, and since from (18) it follows that

$$\tau = \frac{1}{\alpha}[1-(1+t)^{-(\gamma+1)/(\gamma-1)}], \tag{21}$$

and $\gamma > 1$, then the time span $0 \leqslant t < +\infty$ corresponds to $0 \leqslant \tau < \alpha^{-1}$.

The heat transfer at the wall $x = 0$, which is the quantity that we are most interested in, and which is defined by

$$q(t) = -k\left.\frac{\partial T}{\partial x}\right|_{x=0} \tag{22}$$

becomes, upon transforming

$$q(\tau) = -p(\tau)^{\Gamma+1}\left.\frac{\partial \chi}{\partial \psi}\right|_{\psi=0}. \tag{23}$$

Another quantity of interest is the velocity component normal to the walls which is caused by gas expansion. In the streamline coordinate system it is obtained from

$$u(\psi,\tau) = \left.\frac{\mathrm{d}x}{\mathrm{d}t}\right|_{\psi} = \frac{p(\tau)}{Pe}\left.\frac{\mathrm{d}x}{\mathrm{d}\tau}\right|_{\psi}. \tag{24}$$

As will be seen shortly, even in the case where an expression for u can be explicitly written down, it is extremely long and complicated. A fairly good approximation to it can be obtained by realizing that $\partial\rho/\partial t$ in the boundary layer, because of mass continuity, can be approximated by $\partial\rho_1/\partial t$. Then, with the use of equation (8), the continuity equation (10) can be integrated, and using the fact that $u = 0$ at the wall, and using the equation of state (12), we can write

$$u(x,t) \approx \frac{2x}{\gamma-1}(1+t)T(x,t). \tag{25}$$

Note that outside the boundary layer $T(x,t) \approx T_1(t)$, and thus the velocity has the following linear behavior with x:

$$u(x,t) \approx \frac{2x}{\gamma-1}(1+t)^{-1}. \tag{26}$$

We point out that if our vessel were cylindrical in shape and discharged from the center of one end, then the speed of the gas, with the origin located at the opposite end of the cylinder, would be given by equation (26). In this case $V/S_1 = L$, where L is the dimensionless cylinder length. Then we see that at $x = L$ equation (26) matches equation (9) for the speed at surface 1 exactly. We thus obtain the result that, except very near the end wall opposite to the discharge, the speed varies linearly with the coordinate normal to it. A simple correction next to the wall can be provided by equation (25).

3. BOUNDARY-LAYER SOLUTIONS

The solution of the problem posed by (19) and (20) is given by Carslaw and Jaeger [6, p. 63] in the form

$$\chi = \frac{\psi}{2\sqrt{\pi}}\int_0^{\tau}\chi_0(\lambda)\frac{\mathrm{e}^{-\psi^2/4(\tau-\lambda)}}{(\tau-\lambda)^{3/2}}\,\mathrm{d}\lambda. \tag{27}$$

Transforming back to the dimensionless temperature we have

$$T(\psi,\tau)=P(\tau)^{\Gamma}\left[1+\frac{\psi}{2\sqrt{\pi}}\times\int_0^{\tau}\chi_0(\lambda)\frac{e^{-\psi^2/4(\tau-\lambda)}}{(\tau-\lambda)^{3/2}}\,d\lambda\right]. \quad (28)$$

The distance from the wall x is obtained from the definition of the stream function (16) and the solution (28), and can be written in the form

$$x(\psi,\tau)=p(\tau)^{-1/\gamma}\left\{\psi+\frac{1}{\sqrt{\pi}}\left[\int_0^{\tau}\frac{\chi_0(\lambda)}{(\tau-\lambda)^{1/2}}\,d\lambda-\int_0^{\tau}\chi_0(\lambda)\frac{e^{-\psi^2/4(\tau-\lambda)}}{(\tau-\lambda)^{1/2}}\,d\lambda\right]\right\}; \quad (29)$$

the time is obtained from inverting (21).

Now since

$$\left.\frac{\partial\chi}{\partial\psi}\right|_{\psi=0}=-\frac{1}{\sqrt{\pi}}\frac{d}{d\tau}\int_0^{\tau}\frac{\chi_0(\lambda)}{(\tau-\lambda)^{1/2}}\,d\lambda,$$

it can be shown [7, p. 512], using Duhamel's integral, that the heat flux at the wall can be written in the form

$$q(t)=\frac{p(\tau)^{1+\Gamma}}{\sqrt{\pi}}\left[\frac{\chi_0(0)}{\tau^{1/2}}+\int_0^{\tau}\frac{d\chi_0(\lambda)}{d\lambda}(\tau-\lambda)^{-1/2}\,d\lambda\right]. \quad (30)$$

It can be shown, by integrating by parts, that (30) can be written as

$$q(\tau)=\frac{p(\tau)^{1+\Gamma}}{\sqrt{\pi}}\left[\frac{\chi_0(\tau)}{\tau^{1/2}}+\frac{1}{2}\int_0^{\tau}\frac{\chi_0(\tau)-\chi_0(\lambda)}{(\tau-\lambda)^{3/2}}\,d\lambda\right], \quad (31)$$

which is a much more useful formula for experimentalists, since to calculate the heat flux, it does not require any numerical derivatives, but just temperature measurements of the gas next to the walls.

(a) *Explicit solutions*

For given values of the mapped coordinates (ψ, τ) we can explicitly obtain, after much work [8], the following solutions for the temperature

$$T(\psi,\tau)=p(\tau)^{\Gamma}\left[erf\left(\frac{\psi}{2\sqrt{\tau}}\right)+\frac{T_w\psi}{2\sqrt{\pi}}I_1(\psi,\tau)\right]; \quad (32)$$

for the distance from the wall,

$$x(\psi,\tau)=p(\tau)^{-1/\gamma}\left\{\psi\,erf\left(\frac{\psi}{2\sqrt{\tau}}\right)-2\sqrt{\frac{\tau}{\pi}}\times\left[1-e^{-\psi^2/4\tau}-T_w\,{}_2F_1\left(1,2\left(\frac{\gamma-1}{\gamma+1}\right);\frac{3}{2};\alpha\tau\right)\right]-\frac{T_w}{\sqrt{\pi}}I_2(\psi,\tau)\right\}; \quad (33)$$

for time,

$$t(\tau)=(1-\alpha\tau)^{-(\gamma-1)/(\gamma+1)}-1; \quad (34)$$

and for the wall heat flux,

$$q(\tau)=(T_w-1)\frac{p(\tau)^{1+\Gamma}}{\sqrt{\pi\tau}}+4T_w\,Pe\,p(\tau)^{1+\Gamma}\sqrt{\frac{\tau}{\pi}}\times{}_2F_1\left(1,1+2\left(\frac{\gamma-1}{\gamma+1}\right);\frac{3}{2};\alpha\tau\right). \quad (35)$$

In the above equations *erf* stands for the error function, I_1 and I_2 for the integrals

$$I_1(\psi,\tau)=\int_0^{\tau}(1-\alpha\lambda)^{-2(\gamma-1)/(\gamma+1)}\frac{e^{-\psi^2/4(\tau-\lambda)}}{(\tau-\lambda)^{3/2}}\,d\lambda, \quad (36)$$

$$I_2(\psi,\tau)=\int_0^{\tau}(1-\alpha\lambda)^{-2(\gamma-1)/(\gamma+1)}\frac{e^{-\psi^2/4(\tau-\lambda)}}{(\tau-\lambda)^{1/2}}\,d\lambda, \quad (37)$$

and ${}_2F_1$ for Gauss' hypergeometric function which can also be expressed as an infinite series:

$${}_2F_1(1,\varepsilon;\tfrac{3}{2};\alpha\tau)=\frac{\sqrt{\pi}}{2\Gamma(\varepsilon)}\sum_{n=0}^{\infty}\frac{\Gamma(\varepsilon+n)}{\Gamma(\frac{3}{2}+n)}(\alpha\tau)^n, \quad (38)$$

where Γ represents the gamma function. For the convergence conditions of (38) see ref. [8].

Using equations (24), (33), and Duhamel's integral, an explicit solution can also be obtained for the gas expansion speed $u(\psi, \tau)$, but the result is long so it will not be written down. However, we shall plot the results for specific cases in the next section.

One interesting point to note is that the solution for the heat flux (35), unlike that of the temperature (32), does not involve any integrals. Thus explicit values can be obtained by just evaluating Gauss' hypergeometric function.

(b) *Derived quantities*

Other quantities of interest for the particular problem are the Nusselt number Nu, the Rayleigh number Ra, the thermal boundary-layer thickness δ and the boundary layer Rayleigh number Ra_δ.

We define the Nusselt number by

$$Nu(t)=\frac{1}{2}\frac{q(t)}{k_1(T_w-T_1)},$$

and since we have assumed that the thermal conductivity varies linearly with temperature, we can rewrite

$$Nu(t)=\frac{1}{2}\frac{q(t)}{T_1(t)[T_w-T_1(t)]}, \quad (39)$$

where $q(t)$ is given by (34) and (35), and $T_1(t)$ by (8).

Similarly, it can also be shown that the Rayleigh number is given by

$$Ra(t)=\frac{Ra_0}{8}p(t)^2T_1(t)^{-5}[T_w-T_1(t)], \quad (40)$$

where $Ra_0 = Re\,Pe/Fr$. To obtain the above result, we have evaluated all the properties at the core

temperature. Usually, in heat transfer calculations, one is interested in the functional relationship between the Nusselt number and the Rayleigh number. This relationship for our particular problem is given by

$$Nu(t) = \frac{Ra_0}{16} p(t)^2 T_1(t)^{-6} \frac{q(t)}{Ra(t)}. \tag{41}$$

There is a certain degree of arbitrariness in defining a thermal boundary-layer thickness $\delta(t)$. A directly measurable definition, and the one we choose, is given by the locus of points where the temperature is within 1% of the core temperature, that is,

$$\frac{T(x,t)-T_1(t)}{T_w-T_1(t)} = 0.01. \tag{42}$$

Having a measure of $\delta(t)$, we are now in a position to compute the Rayleigh number based on the boundary-layer thickness:

$$Ra_\delta(t) = 8\delta(t)^3\, Ra(t). \tag{43}$$

The above quantity is very important in predicting the time at which the conduction layer will become unstable, and subsequently giving rise to a thermal plume. We shall say more about this later when specific results will be presented.

(c) *Solutions of monatomic gases* ($\gamma = \frac{5}{3}$)

For the case of $\gamma = \frac{5}{3}$ the solutions simplify somewhat, since from [9, p. 1041] we find that

$${}_2F_1(1, \tfrac{1}{2}; \tfrac{3}{2}; \alpha\tau) = \frac{\tanh^{-1}\sqrt{\alpha\tau}}{\sqrt{\alpha\tau}}, \tag{44}$$

and from [10, p. 556] we have that

$${}_2F_1(1, \tfrac{3}{2}; \tfrac{3}{2}; \alpha\tau) = (1-\alpha\tau)^{-1}. \tag{45}$$

The integrals I_1 and I_2 given by (36) and (37) cannot be simplified. The major simplification obtained in this case is that the heat flux at the wall can be written down as a simple function of time:

$$q(t) = 2\sqrt{\frac{Pe}{\pi}}\,(1+t)^{-5}\,\frac{[T_w(1+t)^4-1]}{[(1+t)^4-1]^{1/2}}. \tag{46}$$

To obtain the above equations we have substituted equations (8), (21) and (45) into equation (35).

(d) *Solutions for gases with extremely complex molecules* ($\gamma \approx 1$)

Extremely complex molecules, such as freon and gaseous compounds of uranium have values of γ only slightly larger than unity. For such gases, solutions having a much simpler form can be obtained.

To obtain the boundary-layer solutions, however, we need to obtain the isentropic solutions for $\gamma = 1$. As can be observed, the solutions (8) and (9), and the reference time $\mathscr{T}$, are singular for this case. To remove the singularity, the reference time is redefined to $\mathscr{T}^{-1} = S_2^* c_0 r/V^*$, where in this case it can be easily shown that the critical pressure ratio is given by $r = e^{-1/2}$. Then the isentropic solutions can be obtained by taking the limits of (8) and (9), and are given by

$$T_1 = 1, \quad p_1 = \rho_1 = e^{-t}. \tag{47}$$

The mass flow-rate and the velocity at surface 1 are now given by

$$\dot{m} = V e^{-t}, \quad v_1 = \frac{V}{S_1}. \tag{48}$$

Note that in this case the velocity at surface 1 is constant as long as the flow remains choked, that is, until $p_a/p_1 < e^{-1/2}$ remains valid.

We now observe that in this case $\chi_0(\tau) = T_w - 1$, and the solutions become (see [8]):

$$T(\psi,\tau) = 1 + (T_w-1)\, erfc\left(\frac{\psi}{2\sqrt{\tau}}\right), \tag{49}$$

$$x(\psi,\tau) = p(\tau)^{-1}\left\{\psi + \frac{(T_w-1)}{\sqrt{\pi}}\left[2\sqrt{\tau}\,(1-e^{-\psi^2/4\tau}) + \sqrt{\pi}\psi\, erfc\left(\frac{\psi}{2\sqrt{\tau}}\right)\right]\right\}, \tag{50}$$

$$t(\tau) = -\ln(1-Pe\,\tau), \tag{51}$$

$$q(\tau) = \frac{(T_w-1)p(\tau)}{\sqrt{\pi\tau}}, \tag{52}$$

$$u(\psi,\tau) = x(\psi,\tau) + \frac{(T_w-1)p(\tau)^{-1}}{\sqrt{\pi\tau}}\,(1-e^{-\psi^2/4\tau}). \tag{53}$$

In this case also the heat flux at the wall can be written explicitly in terms of the new dimensionless time

$$q(t) = (T_w-1)\,e^{-t}\sqrt{\frac{Pe}{\pi(1-e^{-t})}}. \tag{54}$$

The form of (54) for $\gamma = 1$ is entirely different than the form of (46) for $\gamma = 5/3$, thus explaining the author's inability to write the heat flux for the case $\gamma = 7/5$ in a form simpler than that given by (35).

A very interesting result for the special case of $\gamma = 1$ is that the boundary-layer thickness can be expressed in a simple form. Using the result (49), and the definition for boundary-layer thickness (42), an expression for ψ in terms of τ can be obtained, which after substitution in (50), and using the transformation (51), ultimately yields the following expression:

$$\delta(t) = [3.64282 + 1.12391(T_w-1)]\sqrt{\frac{1-e^{-t}}{Pe}}. \tag{55}$$

For completeness, the approximate equation for the speed in the boundary layer, equivalent to (25), but for $\gamma = 1$, is given by

$$u(x,t) \approx xT(x,t), \tag{56}$$

and since in this case $T(x,t) \approx 1$ outside the boundary layer, we then have that $u(x,t) \approx x$ there. Observe that at $x = L$, $u = L$, matching exactly with equation (48), at surface 1 for the cylinder discharge described earlier.

Note that the solution to the pure heat conduction problem where $p(t) = 1$ can be obtained from the above solutions by substituting unity for $p(\tau)$ and replacing equation (51) by $t(\tau) = Pe\,\tau$.

(e) *Solutions for small time and* $\gamma > 1$

It is easy to show that for $T_w = 1$ and

$$t < \left[1 - 0.2\left(\frac{\gamma+1}{3\gamma-1}\right)\right]^{-(\gamma-1)/(\gamma+1)} - 1, \quad (57)$$

we can write

$$\chi_0(\tau) \approx 2Pe\,\tau, \quad (58)$$

with less than 10% error. In this case we can write the solutions in a simpler form for arbitrary $\gamma > 1$. The results can be shown to be (see [8]):

$$T(\psi,\tau) = p(\tau)^{\Gamma}\left\{1 + 2Pe\,\tau\left[\left(1 + \frac{\psi^2}{2\tau}\right) \times erfc\left(\frac{\psi}{2\sqrt{\tau}}\right) - \frac{\psi}{\sqrt{\pi\tau}}\,e^{-\psi^2/4\tau}\right]\right\}, \quad (59)$$

$$x(\psi,\tau) = p(\tau)^{\Gamma-1}\left\{\psi + \frac{8}{3}\frac{Pe}{\sqrt{\pi}}\tau^{3/2}\left[1 - \left(1 + \frac{\psi^2}{4\tau}\right) \times e^{-\psi^2/4\tau} + \sqrt{\pi}\,\frac{\psi}{4\sqrt{\tau}}\left(3 + \frac{\psi^2}{2\tau}\right) erfc\left(\frac{\psi}{2\sqrt{\tau}}\right)\right]\right\}, \quad (60)$$

$$t(\tau) = \left[1 - Pe\left(\frac{\gamma+1}{\gamma-1}\right)\tau\right]^{-(\gamma-1)/(\gamma+1)} - 1, \quad (61)$$

$$q(\tau) = 4Pe\,p(\tau)^{1+\Gamma}\sqrt{\frac{\tau}{\pi}}. \quad (62)$$

An expression for $u(\psi,\tau)$ can also be written, but we shall not write it down here, because it is fairly long. Note that the solution (62) for the wall heat flux is given by (35) with $T_w = 1$, and nothing more than the first term in the series expansion of Gauss' hypergeometric function given by (38).

In this case also, we can express the heat flux at the wall (62) in a simple form as a function of the dimensionless time

$$q(t) = 4(1+t)^{-2(2\gamma-1)/(\gamma-1)} \times \sqrt{\frac{Pe}{\pi}\left(\frac{\gamma-1}{\gamma+1}\right)[1-(1+t)^{-(\gamma+1)/(\gamma-1)}]}. \quad (63)$$

We note again that the above equations guarantee a 10% accuracy only for times satisfying (57): specifically, $t < 0.036$ for $\gamma = 5/3$, or $t < 0.027$ for $\gamma = 7/5$.

4. RESULTS

In this section the behavior of the solutions will be made more evident by displaying them graphically. At the same time we will, whenever possible, compare our results with available experimental and numerical data. We note, however, that the average temperature used in our definition of the Nusselt numbers and Rayleigh numbers, and those used in the experimental and numerical results, differ. We use the isentropic core temperature, instead of the mass-averaged temperature for the whole vessel (which includes the boundary layer). This difference is small during the early discharge. We also mention that the singular integrals (36) and (37), needed in the computations of temperature and normal distance from the wall, were numerically integrated using the subroutine D01AJF in the NAG numerical library [11].

Results from two different experiments, one with nitrogen and the other with helium, have been documented by Johnston and Dwyer [3]. The parameters in the experiments were such as to give $\mathscr{T} = 1.994$ s, $\gamma = 7/5$, $Pe = 4.314 \times 10^3$, and $Ra_0 = 6.659 \times 10^9$ for the nitrogen case, and $\mathscr{T} = 0.434$ s, $\gamma = 5/3$, $Pe = 2.397 \times 10^3$, and $Ra_0 = 1.049 \times 10^8$ for the helium case. Johnston and Dwyer noted that the flows unchoked at a dimensionless time of $t \approx 0.29$ and $t \approx 0.43$, in the nitrogen and helium experiments, respectively. In both cases the wall temperatures remained approximately constant through the experiments. Note that since from our isentropic solutions (8) we can obtain the isentropic discharge times of $t = 0.224$, and $t = 0.306$, for the two cases, respectively, then we can estimate the average loss coefficients, over the time span of interest, from the ratio of isentropic to experimental discharge times. The results are $c_d \approx 0.773$, and $c_d \approx 0.712$, for the nitrogen and helium experiments, respectively. As mentioned previously, the above loss coefficients can be incorporated into our analytical results. The net effect is purely a shift along the time axis.

Because of the lack of experimental data for some parameters, and as a further check on the present results, the author numerically solved the full equations (1)–(4) for the equivalent two-dimensional nitrogen discharge experiment performed by Johnston and Dwyer [3], and described above. The numerical technique used and the algorithm have been previously described elsewhere [12]. The gas was discharged from the center of the top wall in a square vessel through an isentropic nozzle. The solution was obtained for times much longer than those where our early discharge solutions are valid. The time for the flow to unchoke was observed to be 0.226, in very close agreement with the case where the core is isentropic.

Recently Meyer (personal communication) obtained transient Nusselt number results for nitrogen discharging from a 0.3175-cm-diameter opening located on one end of a scuba tank whose length, diameter and volume were approximately 28 cm, 16.5 cm, and 12.111 dm^3, respectively. The initial pressure and temperature were 20.41 atm, and 308.6 K, respectively. The results were obtained by the transient PVT method [1]. Throughout the time of interest, the flow remained choked at the opening. The average loss coefficient was not measured but has been estimated to be between 0.7 and 0.9. We note that from the experimental parameters, we approximately have

$\mathscr{T} = 3.369 \times 10^1$ s, $\gamma = 7/5$, $Pe = 7.652 \times 10^2$, and $Ra_0 = 5.342 \times 10^{10}$ in this case.

(a) *Temperature*

In Figs. 2(a) and (b) we show the temperature profiles, obtained from equations (32)–(34), for different times for the two experiments reported by Johnston and Dwyer [3]. Superposed on the figures are the loci of the boundary-layer thickness as defined by equation (42). It should be noted that even though the nitrogen and helium results are different, because of the differences in the governing parameters, the behaviors are similar qualitatively. No such temperature results are available experimentally; however, the solution from the two-dimensional computation falls almost exactly on top of the curves displayed in Fig. 2(a). We do not display those results for clarity.

(b) *Wall heat flux*

In Figs. 3(a) and (b) we plot equation (35) for the wall heat flux for the nitrogen and helium experiments, respectively. The behavior as a function of time for the helium case can be seen very clearly by looking at the simpler equation (46). Again note the qualitative

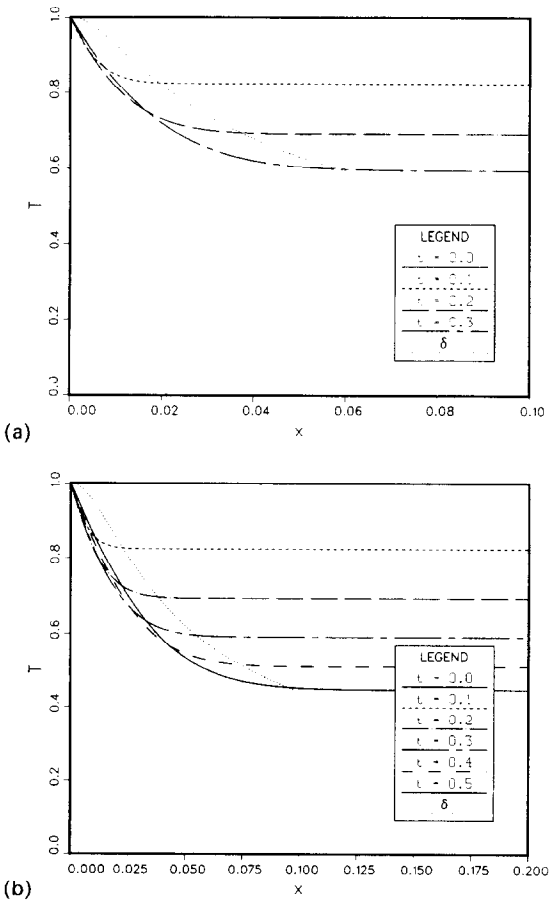

FIG. 2. Temperature profiles in the boundary layer at different times in the (a) nitrogen and (b) helium discharge cases. The dotted lines denote the boundary-layer thicknesses.

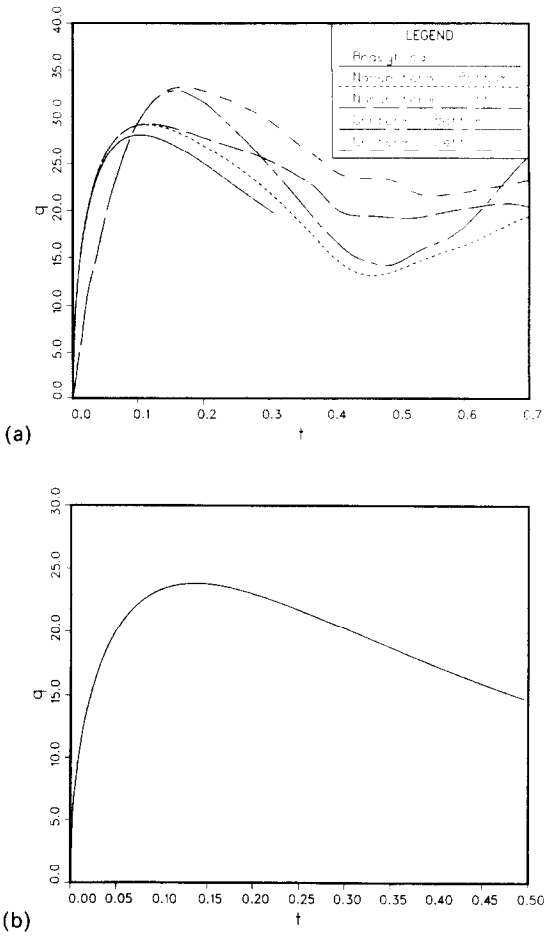

FIG. 3. Wall heat fluxes as functions of time in the (a) nitrogen and (b) helium discharge cases.

similarity between the two cases. The major difference being that in the nitrogen case the rate of heat transfer is substantially higher, and it peaks at a higher value than the helium case. No experimental data is available for the wall heat flux. In order to obtain accurate experimental data, it is obvious that one needs to instrument the experiment for a fast response time.

In Fig. 3(a) we also show numerical results using 91 grid points in each of the two coordinate directions. In one case the grids were uniform, in the other they were nonuniform with high grid refinement next to the walls as described in [12] (the ratio between the smallest and largest grid present was 0.0654). For each case we show the average heat flux on the bottom and left walls. The result for the right wall is the same as that for the left due to the symmetry of the problem. For the top wall the solution is somewhat higher than the left wall only after the branching.

There are a few things that are evident from the results. First, we see that even with a total of 8281 grid points, we do not have enough resolution next to the walls. When the grids are made nonuniform, we see that the solution in the early stages converges to our analytical solution. But even in this case, the grids were

determined not to be fine enough next to the walls. Second, we observe that at $t \approx 0.2$ the effects of natural convection start to become important. This is evident from the branching out in the values of the heat flux. At a time later than $t = 0.7$, the average heat flux for the entire vessel will peak again due to the effects of buoyancy in generating vigorous motions. A feature of the average wall heat flux history, which to the author's knowledge has not been previously observed, is the presence of two distinct peaks; an early one due to conduction, and a later one due to natural convection. It is conceivable that for a different set of parameters the conduction and convection peaks could be much closer, and subsequently only one peak would be experimentally observable.

(c) *Boundary-layer thickness*

We next show the boundary-layer thickness in Figs. 4(a) and (b) corresponding to the two experiments of Johnston and Dwyer [3]. In this case we can make a few comparisons with published results. For both experiments we plot our analytical results, the similarity solution obtained by Landram [2] (as corrected by Johnston and Dwyer [3]), the numerical solution obtained by Johnston and Dwyer [3], together with their experimental data. For the nitrogen case we also display the boundary-layer thickness measured from the center bottom wall obtained from the two-dimensional numerical simulation.

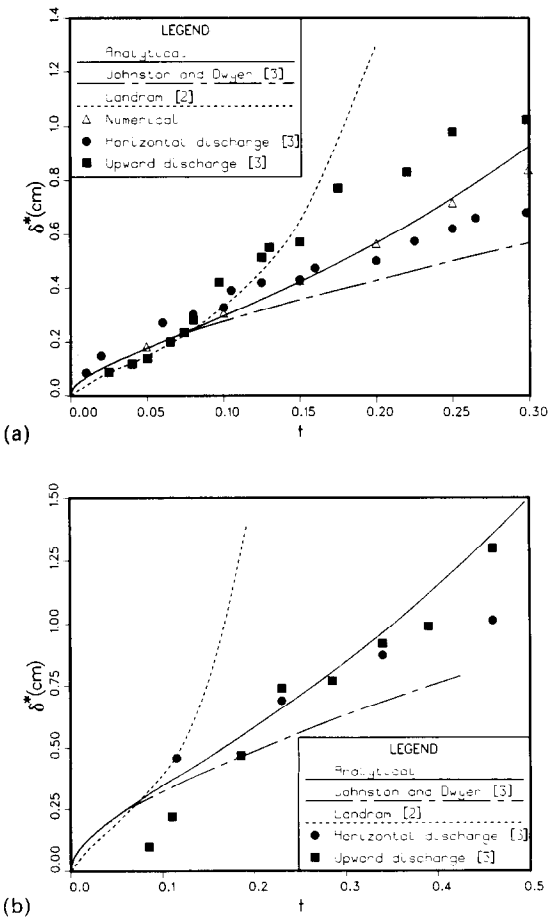

FIG. 4. Boundary-layer thicknesses as functions of time in the (a) nitrogen and (b) helium discharge cases.

As noted before, and as Johnston and Dwyer point out, Landram assumes a similarity solution in obtaining his results. Clearly the solutions that we obtained are not similar, hence explaining the incorrect behavior of Landram's results for all values of time.

On the other hand, Johnston and Dwyer's numerical results agree with our results only at very small times. For times larger than 0.07 for the nitrogen case, and 0.05 for the helium case, their results diverge from our analytical solution. The differences can be easily explained. At very early times, because of the inertia, the gas in the boundary layer has not had enough time to respond to the incoming heat, hence the heat transfer is due to pure heat conduction, with no convection. During this time our analytical solution yields the same results as Johnston and Dwyer's numerical heat conduction solutions. At later times the gas in the boundary layer expands, thus giving rise to convective effects. The differences in the boundary-layer thickness measure directly the effects of gas expansion. Without this expansion, the wall heat fluxes shown in Figs. 3(a) and (b) would not have relative maxima, but would keep increasing indefinitely. Thus the peak observed in the wall heat flux is due solely to the gas expansion in the boundary layer. We note that the value of δ that we show is based on the conventional definition of 99% attainment of the core gas temperature far from the walls. The δ obtained by Johnston and Dwyer, instead, corresponds to 99.5% attainment, while that obtained from Landram's integral method is based on an approximating polynomial. Since the definitions are not the same, it would appear that the comparisons are unfair. However, the author has found that bringing the three results on the same basis produced no discernible differences from the results shown in Figs. 4(a) and (b).

Johnston and Dwyer also obtained experimental results from measurements of schlieren photographs at the 7 o'clock position on their cylinder for three discharge orientations: top, bottom, and side. Since the 7 o'clock position is too close to the opening for the bottom discharge case, it is felt that those measurements would not make a good test for the theory. Hence only their top and side discharge boundary-layer thickness results have been plotted. We also note that since the results were obtained from visual inspection of schlieren photographs, one cannot say for certain what percentage attainment of the core temperature the results correspond to, and also for this very reason one cannot apply a consistent definition at different values of time, or for different experiments. Hence the considerable scatter in their data, as evident by looking at the data points in Figs. 4(a) and (b), is understandable. The most that can be said is that the data scatters about our analytical solutions.

As is evident from Fig. 4(a), the result from the two-

dimensional numerical simulation is in excellent agreement with our analytical result. We also observe from the figure that the two results only start deviating at $t \approx 0.25$. The difference in the results between $t \approx 0.25$ and $t \approx 0.30$ is due to buoyancy effects which were neglected in our analysis, and to the change in mass flow rate since after $t = 0.226$ the flow is unchoked.

(d) *Boundary-layer Rayleigh number*

In Figs. 5(a) and (b) we show the Rayleigh number based on the boundary-layer thickness Ra_δ as given by equation (43) for the two cases. Superposed on the figures are the results of Johnston and Dwyer [3] for the top and side discharge, and of our two-dimensional simulation. The viscosity, thermal diffusivity, and coefficient of volumetric expansion used in calculating the experimental and numerical Rayleigh numbers have been evaluated at the measured and computed mass-averaged gas temperatures. In distinction, in our analysis the above quantities are evaluated at the core temperature. The two temperatures should remain fairly close for small times and start departing from each other when either the boundary layer becomes unstable, or when the total volume enclosed by the boundary layer exceeds approx. 10% of the total volume of the vessel.

Note from the figures that the behaviors of the experimental and analytical results are much alike. However, the two quantitative results differ substantially. This can be attributed to two effects. First, since the Rayleigh number is proportional to the third power of the boundary-layer thickness, it is evident by looking at Figs. 4(a) and (b) that one could not expect good quantitative agreement. Second, the actual discharge is not exactly isentropic. Had a constant total loss coefficient been included through the time scaling, the net result would have been to shift the experimental data points to the left of those shown in Figs. 5(a) and (b). This would have yielded better agreement with the analytical results.

In contrast, by looking at Fig. 5(a), one can see that

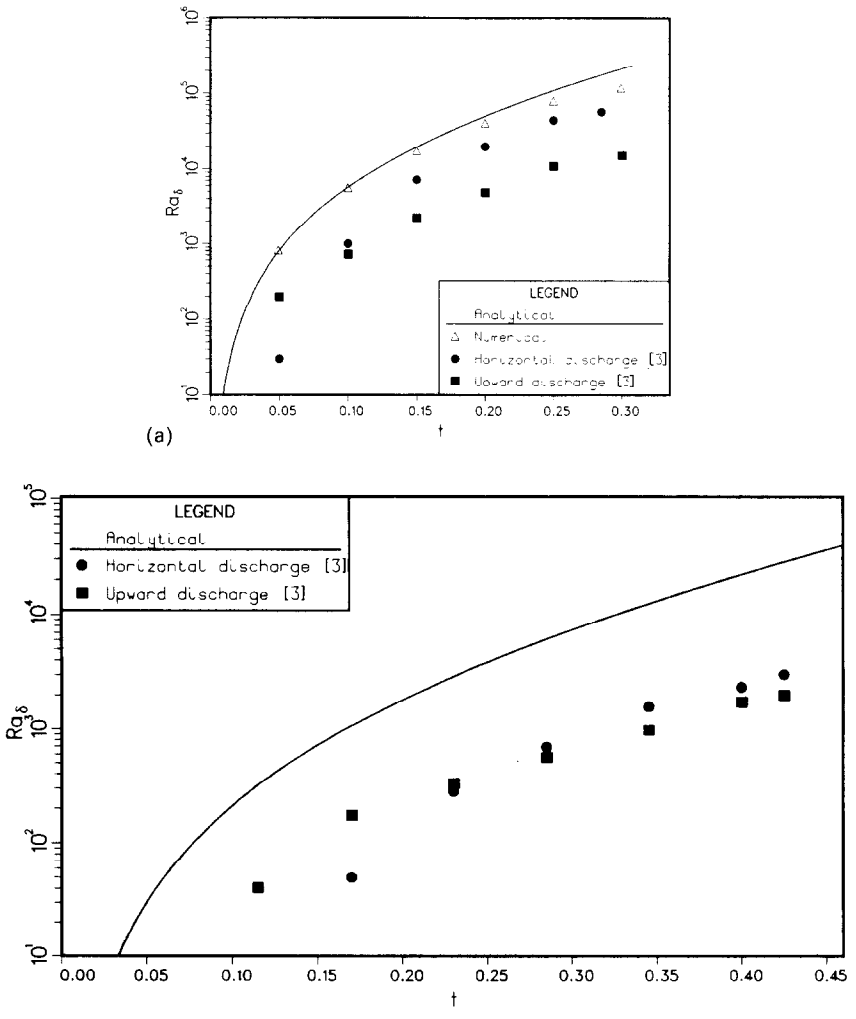

FIG. 5. Boundary-layer Rayleigh numbers as functions of time in the (a) nitrogen and (b) helium discharge cases.

the agreement between the analytical result and the numerical simulation is excellent. The two results start deviating somewhat from each other at the approximate time of 0.25 due to increasing buoyancy effects, and since the flow becomes unchoked at $t = 0.226$.

A very important result which could be obtained from the variation of the boundary-layer Rayleigh number is the approximate time at which the boundary layer would become unstable and thus give rise to a thermal plume (or plumes). This of course would occur on the bottom of the vessel because of a buoyant instability (note that this may not occur if the discharge opening is at the bottom of the vessel, since in this case the boundary layer would be sucked out). Unfortunately no stability analysis has been performed to date on this highly transient problem. This would involve looking at the stability of a compressible gas in contact with and on top of an infinite wall, where the gas would be cooled in a time dependent fashion. A similar analysis has been performed by Foster [13], but for an incompressible fluid with constant properties and with linear time dependence. His results are clearly not applicable to our particular problem.

Johnston and Dwyer [3], in the case of nitrogen discharge with wall vibrations (induced by an explosively actuated valve), crudely estimated the critical boundary-layer Rayleigh number for instability to be approx. 10^5. If we accept their estimate, then from Fig. 5(a) we predict the estimated time for the instability to occur is ~ 0.24. This time is very close to the values of 0.25 and 0.30 which Johnston and Dwyer estimated for the top and side discharge orientations, respectively. No instability was observed in the downward discharge case since, as pointed out, the boundary layer at the point of maximum potential instability is sucked out. Johnston and Dwyer also point out that with no wall vibrations they noted an instability formation for the top discharge case at the approximate time of 0.45. This suggests that the stability map for our problem might be subcritical. That is, for a large enough perturbation amplitude, the system might become unstable at a lower Rayleigh number than the critical Rayleigh number obtained from a linear analysis with perturbations of infinitesimal amplitudes. No instability was observed in the helium experiments, and none would be predicted within the time our results are valid [see Fig. 5(b)] if in this case the critical Rayleigh number for finite amplitude perturbations is $\sim 10^5$ also.

(e) *Gas expansion speed*

Figure 6 shows the speed of the gas normal to the wall as a function of the coordinate normal to the wall, as given by equation (24). Results are shown for both the nitrogen and helium cases, and for two different times. Note that equation (25) is an excellent approximation to the results. Also note that as we move outside the boundary layer (whose thickness is denoted on the curves) the results approach a slope of $2/(\gamma-1)(1+t)^{-1}$,

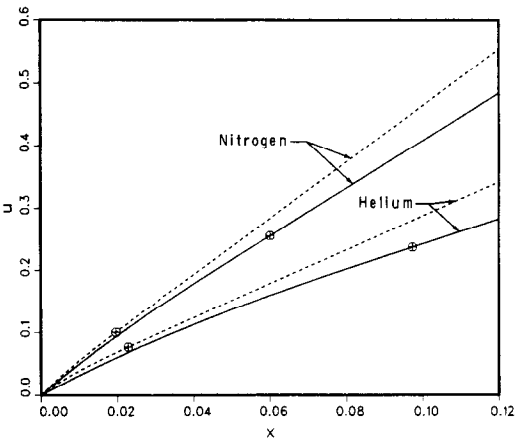

FIG. 6. Gas expansion speed near the vessel boundary at different times. The crosses denote the boundary-layer thickness.

as given by equation (26). At the edge of the boundary layer the velocity is reoriented so as to point directly towards the opening. Of course for a wall whose normal is opposite to the normal vector in the plane of the opening, no reorientation is needed.

The expansion speed results within the boundary layer, obtained from the two-dimensional simulation, are in excellent agreement with the analytical results. Also the speed normal to the center of the bottom wall indeed matches very well with our analytical result, for the nitrogen case, all the way up to the opening. These results are not displayed so as to keep Fig. 6 uncluttered.

(f) *Nusselt number*

Both analytical and experimental Nusselt number histories are shown in Fig. 7. The analytical result was obtained from equation (39) with the wall heat flux calculated from (35). The experimental result was

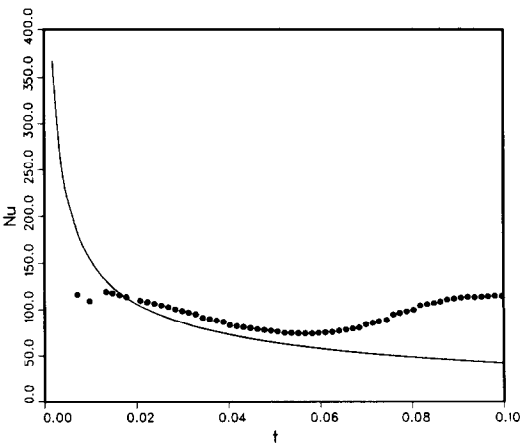

FIG. 7. Nusselt number as a function of time in the nitrogen discharge case corresponding to Meyer's experiment.

obtained from unpublished work of Meyer, as pointed out earlier.

There are three things worth noting here. First, it can be seen from the figure that the response of the instrumentation was not fast enough to pick up the Nusselt number at the very early time. Second, between the nondimensional times of 0.02 and 0.05, the two results are parallel and fairly close to each other. If the estimated constant loss coefficient of 0.8 is incorporated in the time scaling, the experimental data for times between 0.02 and 0.05 falls very close to the analytical result. Third, we notice that for times past 0.05, natural convection starts becoming important, and hence, the experimental Nusselt number starts turning upwards again. Of course the present analysis cannot predict this effect.

5. CONCLUSIONS

At this stage we would like to conclude by summarizing the present work. We have seen that for the problem of gas discharge from a pressurized vessel, if we assume, for early time, that the gas in the wall boundary layer expands normal to the walls, we were able to obtain analytical solutions for its behavior. The most important result obtained is our ability to write down in simple closed form the heat flux at the wall as a function of the parameters governing the problem. To obtain the results, we have made some key assumptions that we shall discuss.

A crucial assumption of the analysis is that the thermal conductivity behaves linearly with temperature. For most gases this assumption is a good one. Johnston and Dwyer [3] used a heat conduction variation of T^n, with $n = 3/4$ in their numerical experiments. They noted that the results they obtained were found to be weak functions of n. This insensitivity can also be seen by the excellent agreement between our boundary-layer thickness results and theirs during the very early time, as displayed in Figs. 4(a) and (b).

Another critical assumption is that the gas in the boundary layer moves normal to the walls during the early part of the discharge. As we observed from the two-dimensional simulation, this was essentially true. The gas only feels the location of the opening once it reaches the edge of the boundary layer, at which point the velocity field is realigned to point towards the opening. Also, the effects of natural convection on this normal velocity and wall heat flux was seen to be negligible during the early stages of the discharge, as clearly illustrated in Figs. 3(a), 4(a) and 5(a).

One important parameter that could not be obtained from the present analysis is the approximate time at which our solutions start to become invalid due to our neglect of buoyancy. As pointed out in the last section, this answer can only be provided from stability considerations, which we hope will become available in the near future. We do note, however, that the upper bound for the time at which our solutions are valid is given by the time at which the flow unchokes. This time can be easily calculated *a priori* for any discharge problem.

Acknowledgement—This work was performed under the auspices of the U.S. Department of Energy by Sandia National Laboratories, Livermore, under contract No. DE-AC04-76DP00789.

REFERENCES

1. S. C. Johnston, A characterization of unsteady gas discharge from a vessel SAND75-8207, Sandia National Laboratories, Livermore, California (1975).
2. C. S. Landram, Heat transfer during vessel discharge: mean and fluctuating gas temperature, *J. Heat Transfer* **95,** 101–106 (1973).
3. S. C. Johnston and H. A. Dwyer, Thermal instabilities in discharging gas reservoirs, *J. Heat Transfer* **98,** 360–366 (1976).
4. S. Paolucci, On the filtering of sound from the Navier–Stokes equations, SAND82-8257, Sandia National Laboratories, Livermore, California (1982).
5. R. Grief, T. Namba and M. Nikanham, Heat transfer during piston compression including side wall and convection effects, *Int. J. Heat Mass Transfer* **22,** 901–907 (1979).
6. H. S. Carslaw and J. C. Jaeger, *Conduction of Heat in Solids*, 2nd edn. Oxford University Press, Oxford (1959).
7. R. Courant and D. Hilbert, *Methods of Mathematical Physics*, Vol. 2. Wiley, New York (1962).
8. S. Paolucci, Heat transfer during the early discharge of gas from pressurized vessels, SAND84-8874, Sandia National Laboratories, Livermore, California (1985).
9. I. S. Gradshteyn and I. M. Ryzhik, *Table of Integrals, Series and Products*. Academic Press, New York (1965).
10. M. Abramowitz and I. A. Stegun, *Handbook of Mathematical Functions*. Dover, New York (1972).
11. Numerical Algorithms Group, NAG Fortran Library Manual, Mark 9, Vol. 1, Oxford (1982).
12. S. Paolucci and D. R. Chenoweth, The effect of forced and free convection in the discharge of a pressurized gas, in *Numerical Methods in Laminar and Turbulent Flow*, C. Taylor and B. A. Schrefler (Editors), pp. 1045–1057. Pineridge Press, Swansea, U.K. (1982).
13. T. D. Foster, Effect of boundary conditions on the onset of convection, *Phys. Fluids* **11,** 1257–1262 (1968).

TRANSFERT THERMIQUE PENDANT LE DEBUT DE LA DETENTE D'UN GAZ DANS UN RESERVOIR SOUS PRESSION

Résumé—On étudie le comportement d'un gaz dans un réservoir pressurisé pendant le début de la détente, dans le cas spécial où il y a un écoulement externe avec choc. En utilisant une approximation de couche limite qui inclut les effets de la conduction et de la détente du gaz, on obtient des solutions analytiques. Le transfert à la paroi est la grandeur-clé qui détermine les mécanismes que le gaz subit au cours de la décharge. A partir des résultats analytiques, on est capable d'identifier les paramètres importants qui gouvernent le début de la détente et particulièrement le mécanisme de transfert thermique.

WÄRMEÜBERGANG WÄHREND DER VOREXPANSION VON GAS IN DRUCKGEFÄSSEN

Zusammenfassung—Es wird das Verhalten eines Gases während der Vorexpansion in einem Druckbehälter untersucht, ehe es diesen bei gedrosselter Strömung verläßt. Durch Verwendung einer Grenzschichtnäherung, die Leitungs- und Gasexpansionseffekte berücksichtigt, kann man analytische Lösungen in geschlossener Form erhalten. Eine maßgebende Größe für die anschließenden Zustandsänderungen, die vom Gas während der folgenden Ausströmphasen durchlaufen werden, ist der Wärmeübergang an die Wand. Aus dem analytischen Ergebnis kann man die wichtigen Parameter feststellen, die für den Ausströmvergang in diesem Anfangsstadium und vor allem für den Wärmeübergang bestimmend sind.

ТЕПЛОПЕРЕНОС НА РАННЕЙ СТАДИИ РАСШИРЕНИЯ ГАЗА В СОСУДАХ ПОД ДАВЛЕНИЕМ

Аннотация—Исследуется поведение газа в сосуде под давлением на ранней стадии расширения для особого случая, в котором истекающий поток дросселируется, Используя приближение пограничного слоя, включающее теплопроводность и эффекты газового расширения, получено аналитическое решение в замкнутом виде. Основной величиной, определяющей последующие процессы, через которые проходит газ на более поздних стадиях разряда, является теплообмен со стенкой. Из аналитических результатов возможно определить основные параметры, характеризующие начальную стадию разряда и, в частности, процесс теплообмена.